J Geod (2014) 88:959–973
DOI 10.1007/s00190-014-0736-6

ORIGINAL ARTICLE

Comparison of GOCE-GPS gravity fields derived by different approaches

O. Baur · H. Bock · E. Höck · A. Jäggi · S. Krauss · T. Mayer-Gürr · T. Reubelt · C. Siemes · N. Zehentner

Received: 1 October 2013 / Accepted: 28 May 2014 / Published online: 20 June 2014

Abstract Several techniques have been proposed to exploit GNSS-derived kinematic orbit information for the determination of long-wavelength gravity field features. These methods include the (i) celestial mechanics approach, (ii) short-arc approach, (iii) point-wise acceleration approach, (iv) averaged acceleration approach, and (v) energy balance approach. Although there is a general consensus that—except for energy balance—these methods theoretically provide equivalent results, real data gravity field solutions from kinematic orbit analysis have never been evaluated against each other within a consistent data processing environment. This contribution strives to close this gap. Target consistency criteria for our study are the input data sets, period of investigation, spherical harmonic resolution, a priori gravity field information, etc. We compare GOCE gravity field estimates based on the aforementioned approaches as computed at the Graz University of Technology, the University of Bern, the University of Stuttgart/Austrian Academy of Sciences, and by RHEA Systems for the European Space Agency. The involved research groups complied with most of the consistency criterions. Deviations only occur where technical unfeasibility exists. Performance measures include formal errors, differences with respect to a state-of-the-art GRACE gravity field, (cumulative) geoid height differences, and SLR residuals from precise orbit determination of geodetic satellites. We found that for the approaches (i) to (iv), the cumulative geoid height differences at spherical harmonic degree 100 differ by only ≈10 %; in the absence of the polar data gap, SLR residuals agree by ≈96 %. From our investigations, we conclude that real data analysis results are in agreement with the theoretical considerations concerning the (relative) performance of the different approaches.

Keywords Gravity field · Orbit analysis · Kinematic positions · GOCE · GPS · Comparison of approaches

O. Baur (✉) · E. Höck · S. Krauss
Space Research Institute, Austrian Academy of Sciences,
Schmiedlstr. 6, 8042 Graz, Austria
e-mail: oliver.baur@oeaw.ac.at

E. Höck
e-mail: eduard.hoeck@oeaw.ac.at

S. Krauss
e-mail: sandro.krauss@oeaw.ac.at

H. Bock · A. Jäggi
Astronomical Institute, University of Bern,
Sidlerstrasse 5, 3012 Bern, Switzerland
e-mail: heike.bock@aiub.unibe.ch

A. Jäggi
e-mail: adrian.jaeggi@aiub.unibe.ch

T. Mayer-Gürr · N. Zehentner
Institute of Theoretical Geodesy and Satellite Geodesy, Graz University of Technology, Steyrergasse 30/III, 8010 Graz, Austria
e-mail: mayer-guerr@tugraz.at

N. Zehentner
e-mail: zehentner@tugraz.at

T. Reubelt
Institute of Geodesy, University of Stuttgart, Geschwister-Scholl-Str. 24D, 70174 Stuttgart, Germany
e-mail: reubelt@gis.uni-stuttgart.de

C. Siemes
RHEA for ESA-European Space Agency,
Keplerlaan 1, 2200 AG Noordwijk, The Netherlands
e-mail: christian.siemes@esa.int

1 Introduction

The direct analysis of tracking data of artificial satellites orbiting the Earth is one of the oldest techniques to determine the terrestrial gravity field from space. Initially, this task was accomplished by solving the satellite's equation of

motion based on laser and Doppler measurements (dynamic orbit computation). This common practice has changed fundamentally since Global Navigation Satellite Systems (GNSS)—such as the Global Positioning System (GPS)—can be used now for precise orbit determination. In contrast to the dynamic approach, GNSS allow epoch-wise purely geometric spacecraft positioning. These so-called kinematic orbits circumvent the adoption of force models, and hence are independent of a priori gravity field information. Kinematic orbits may be considered as "auxiliary products". A more stringent way would be to infer gravitational features from GNSS measurements directly. The direct analysis of GNSS data and the analysis of kinematic orbits yield equivalent gravity field solutions if and only if the full correlations between the kinematic positions are taken into account (cf. Jäggi et al. 2011a).

Nowadays, low Earth orbiters (LEOs) are routinely tracked by GPS; the observation principle is known as Satellite-to-Satellite Tracking in the high-low mode (SST-hl). Kinematic orbits have first been provided for the CHAllenging Mini-satellite Payload (CHAMP) mission (cf. Švehla and Rothacher 2002, 2004); processing up to 8 years of GPS measurements, the gravity field could be recovered up to spherical harmonic degree and order (d/o) ≈100 (e.g., Flechtner et al. 2010; Prange 2011).

It has to be emphasized that only long-wavelength gravitational features can be recovered by SST-hl, which is due to the strong attenuation of the geopotential signal with altitude (Meissl 1971). For this reason, stand-alone SST-hl analysis is not very well pronounced for the Gravity Recovery And Climate Experiment (GRACE) project. The key GRACE measurements are ranges and range-rates between two spacecraft following each other in the same orbit (Tapley et al. 2004). As far as accuracy and sensitivity of most gravity field coefficients are concerned, these inter-satellite observations are superior to orbit perturbations from SST-hl; therefore, GNSS information is down-weighted to have less impact on gravity field determination. This does not hold true for the Gravity field and steady-state Ocean Circulation Explorer (GOCE) mission. GOCE's core instrument—a three-dimensional gravity gradiometer (ESA 1999)—is characterized by a limited measurement bandwidth with a lower bound roughly corresponding to d/o 25 in terms of spherical harmonics. For this reason, satellite gravity gradiometry has to be supplemented by orbit analysis in order to meet one of the ESA's key objectives in the framework of GOCE data analysis, namely the provision of a high-accurate GOCE-only gravity field solution over the entire spectrum (cf. Pail et al. 2011).

In the last decade, several methods have been developed and applied to derive gravity field models from kinematic satellite orbits. These techniques include the (i) energy balance approach (e.g., Han et al. 2002; Gerlach et al. 2003; Badura et al. 2006; Weigelt 2007), hereafter abbreviated EBA; (ii) point-wise acceleration approach (Reubelt et al. 2003; Reubelt 2009), PAA; (iii) averaged acceleration approach (Ditmar and van Eck van der Sluijs 2004), AAA; (iv) short-arc approach (Mayer-Gürr 2006), SAA; (v) celestial mechanics approach (Prange et al. 2009; Beutler et al. 2010a, b), CMA. The theoretical framework of these approaches has been dealt with in a huge number of earlier publications (many references are provided in this paper). In this contribution, for the first time, we assess the relative performance of the approaches with regard to gravity field solutions based on real data. We compare gravity field models obtained from the analysis of the kinematic GOCE orbit. As such, this investigation is motivated against the background of GOCE-only gravity field recovery. However, the results of the study are valid in a more general context. It should be kept in mind that in the absence of GRACE and GOCE, SST-hl will be the primary gravity field inference technique.

The gravity field models used in this study have been computed at the Institute of Navigation and Satellite Geodesy (EBA) and the Institute of Theoretical Geodesy and Satellite Geodesy (SAA) of the Graz University of Technology, the Institute of Geodesy (PAA) of the University of Stuttgart, the Astronomical Institute (CMA) of the University of Bern, and by RHEA Systems for the European Space Agency (AAA).

2 Data

The GOCE satellite (cf. Drinkwater et al. 2007) was launched with a Rockot on March 17, 2009. Since the begin of the Measurement and Operational Phase (MOP) in autumn 2009, the on-board sensors have been collecting science data; the spacecraft was continuously tracked by GPS. The nominal mission duration was 1 year; however, in reality the lifetime could be extended to more than 4 years, which was owing to less fuel consumption as initially expected. Starting in August 2012, the orbit has been lowered in several steps from 255 to 225 km (reached end of May 2013). The end of mission was in November 2013, when GOCE reentered the Earth's atmosphere.

GOCE precise science orbits are delivered within the ESA SST_PSO_2 product (EGG-C 2010). The product contains both kinematic (SST_PKI_2) and reduced-dynamic (SST_PRD_2) orbits. For this investigation, we made use of the 1-s kinematic GOCE orbit, i.e., unconstrained satellite position estimates for each observation epoch (Bock et al. 2011). Position variance-covariance information (SST_PCV_2 product) including full correlation information over four successive epochs is provided together with the kinematic orbit positions. We analyzed the kinematic orbit over the periods (a) November 1, 2009 to January 11, 2010, and (b) November 1, 2009 to July 5, 2010. These periods (denoted

as R1 and R2 in the sequel) are in accordance with the time spans used for the computation of the release 1 and release 2 gravity fields by the GOCE High-level Processing Facility (ESA 2011). We considered two periods in order to investigate whether the results are "robust" against the data time span.

The GOCE satellite was kept in drag-free control in along-track direction, i.e., non-gravitational forces (mainly air drag) were compensated to a large extent. Remaining residual disturbances can be derived from the gradiometer instrument readings. These so-called common mode accelerometer data are provided within the EGG_NOM_1b product (EGG_CCD_2c sub-product; EGG-C 2006); the rotation between the inertial reference frame and the satellite-fixed reference frame was taken from the EGG_IAQ_2c product. Non-tidal atmospheric and oceanic time-variable gravity field information is delivered within the SST_AUX_2 product (EGG-C 2010).

3 Consistency issues

Meaningful evaluation of different analysis approaches via the comparison of gravity field solutions requires consistent data processing. Otherwise, differences between the estimates might be erroneously attributed to method performance rather than to deviations of the adopted processing standards. Table 1 highlights the consistency aspects considered in this study. The background models account for third-body forces, solid Earth tides, ocean tides, solid Earth pole tide, ocean pole tide, atmospheric tides, relativistic corrections, and non-tidal short-term fluctuations. From a series of tests, it turned out that the choice of the ocean tide model is uncritical (not shown here); the same holds true for the non-tidal short-term gravity field variations. The latter can even be neglected in the analysis (not shown here). Some approaches incorporate a priori gravity field information based on the EGM96 model (Lemoine et al. 1998); the choice for this (out-dated) model is to exclude any dependencies of our GOCE-GPS solutions on existing gravity field knowledge.

The CMA and EBA implementations consider the full position variance-covariance information as provided by the SST_PCV_2 product. For SAA, the inner-epoch variance-covariance information was incorporated, whereas temporal correlations were modeled by an empirical covariance function (cf. Sect. 4.2). The PAA estimates include inner-epoch covariance information only; inter-epoch correlations were neglected. The AAA implementation does not make use of any of the provided variance-covariance information but is based on the empirical modeling of both inner-epoch and inter-epoch correlations (cf. Sect. 4.4). For EBA, the spectral resolution (maximum spherical harmonic degree) is 100 compared to 130 for the other approaches. This is due to the fact that no higher resolution EBA gravity fields are available/compilable to date (simultaneously meeting the further consistency issues). The EBA estimates used in this study are the official ESA SST-hl solutions included in the first two releases of the GOCE-only time-wise (GOCE-TIM) gravity field models (Pail et al. 2011).

Extending the parameterization by empirical models is a well-known strategy to cope with the impact of insufficiently modeled/measured perturbing forces. We refrained from a consistent setup of empirical parameters as it turned out that the approaches react differently on the choice of these parameters. Indeed, the method-specific choice of the empirical parameters is somewhat heuristic—one may say the best setup is found by trial and error. We decided the solutions not to be "corrupted" by a sub-optimal selection (as would be the case for some approaches if a consistent setup would be enforced).

Concerning the remaining inconsistencies, it should be noted that each group involved in this study has its own "tradition" how to apply their approach for the inference of gravity field information from kinematic orbits. We put effort into a joint strategy and to process the data as consistently as possible. However, there are limitations to such an endeavor—especially as far as laborious additional implementation is concerned that would improve consistency but is very unlikely to affect the quality of the solutions. For instance, as shown by Reubelt et al. (2013), in case of the PAA the consideration of the provided inter-epoch correlations has no benefit for the GOCE-GPS gravity field solutions.

4 Data processing

This section briefly introduces the orbit analysis approaches underlying the investigated GOCE-GPS gravity fields. We want to emphasize that the focus in the following subsections is on the processing strategies for real data handling; methodological details can be found in the cited literature.

Making use of Newton's equation of motion in the inertial space

$$\mathbf{a}(t) = \mathbf{f}(t, \mathbf{r}, \dot{\mathbf{r}}) = \mathbf{g}(t) + \mathbf{a}_{\mathrm{d}}(t) \tag{1}$$

the acceleration of a satellite, $\mathbf{a}(t)$, is equal to the Earth's gravitational attraction on the spacecraft, $\mathbf{g}(t) = \nabla V(t)$ ($V(t)$ denotes the geopotential). However, the acceleration of a satellite is not solely subject to the Earth's gravitational pull, but depends on additional (gravitational and non-gravitational) perturbing forces acting on the spacecraft (third-body forces, solid Earth tides, air drag, solar radiation pressure, etc.; cf. Sect. 3); the effect of these disturbing forces is summarized in $\mathbf{a}_{\mathrm{d}}(t)$. The overall force function—

Table 1 Processing details from the viewpoint of consistency

	CMA	SAA	PAA	EBA	AAA
Period	1.11.2009–11.1.2010 (R1), 1.11.2009–5.7.2010 (R2)				
Orbit data	SST_PKI_2 product (kinematic GOCE orbit)				
Variance-covariance data	SST_PCV_2 product[a]				No
Non-gravitational accelerations	EGG_CCD_2c product				
Background models	According to IERS Conventions 2003/2010				
Spectral resolution	130	130	130	100	130
Regularization	No	No	No	No	No
A priori information	EGM96	EGM96	EGM96	None	None

[a] PAA, SAA: only inner-epoch information considered

dependent on the satellite position $\mathbf{r}(t)$ and satellite velocity $\dot{\mathbf{r}}(t)$—is denoted as $\mathbf{f}(t, \mathbf{r}, \dot{\mathbf{r}})$.

4.1 Celestial mechanics approach (CMA)

The CMA solves the equation of motion, Eq. (1), by numerical integration. The method was successfully applied to SST-hl data from CHAMP (Prange et al. 2009), GRACE (Jäggi et al. 2009), and GOCE (Jäggi et al. 2011b), as well as inter-satellite ranging data from GRACE (Jäggi et al. 2012). Detailed documentation may be found in Beutler et al. (2010a, b).

In the first step, the 1-s kinematic GOCE positions were used to generate a priori orbits by adjusting arc-specific orbit parameters; as initial gravity field information, we used the EGM96 model. Gross errors were detected and eliminated by comparison of the kinematic positions with GOCE reduced-dynamic orbits; the procedure is described in Prange (2011). The overall data analysis period was split into daily arcs, motivated by the fact that the GOCE orbit products are provided as daily data sets.

In addition to the six Keplerian osculating elements, constant and once-per-revolution empirical accelerations were set up per daily arc in the radial, along-track, and cross-track directions. Furthermore, pseudo-stochastic pulses (instantaneous velocity changes; Jäggi et al. 2006) were considered for all three directions with a spacing of 6 min—from a series of earlier studies, the incorporation of these pulses turned out to be well suited for the CMA. The feasible choice of both the empirical parameters and pseudo-stochastic pulses was according to experience from previous investigations (cf. Jäggi et al. 2011b). The positions were weighted according to the provided (inner-epoch and intra-epoch) covariance information.

Based on the a priori orbits, in the second step gravity field recovery was performed in terms of a generalized orbit improvement problem. The actual orbits were expressed as truncated (i.e. linearized) Taylor series with respect to the unknown parameters (arc-specific orbit parameters and spherical harmonic coefficients representing the Earth's gravity field). The normal equations for each (daily) arc have been accumulated into an overall normal equations system. The latter was eventually inverted (least-squares adjustment) to obtain both corrections to the a priori gravity field and the associated covariance information.

4.2 Short-arc approach (SAA)

The SAA is based on the integral equation approach proposed by Schneider (1968) and is described in detail in Mayer-Gürr (2006). The method was successfully applied to compute various gravity field solutions from data provided by recent space gravimetry missions; these models include ITG-CHAMP01 (Mayer-Gürr et al. 2005a) and ITG-GRACE2010 (Mayer-Gürr et al. 2010). The core of the approach is the reformulation of Newton's equation of motion, Eq. (1), as a boundary value problem according to

$$\mathbf{r}(\tau) = \mathbf{r}_\mathrm{A}(1-\tau) + \mathbf{r}_\mathrm{B}\tau - T^2 \int_0^1 K(\tau, \tau')\mathbf{f}(\tau')\mathrm{d}\tau';$$
$$K(\tau, \tau') = \begin{cases} \tau'(1-\tau) & \text{if } \tau' \le \tau \\ \tau(1-\tau') & \text{if } \tau' > \tau \end{cases}. \qquad (2)$$

In Eq. (2), $\mathbf{r}_\mathrm{A}$ and $\mathbf{r}_\mathrm{B}$ are the boundary values, τ denotes normalized time ($\tau \forall [0, 1]$), and $\mathbf{f}(\tau)$ is the specific force function (cf. Eq. (1)). Furthermore, $T = t_\mathrm{B} - t_\mathrm{A}$ holds true, with start time and end time t_A and t_B, respectively.

For the computation of the SAA solutions presented in this study, we split the 1-s kinematic GOCE orbit into arcs with a length of 30 min. The choice of the arc length is somewhat arbitrary. As shown by Mayer-Gürr (2006), it should be at least ≈20 min; restrictions for the upper bound do not exist. From experience, 30 min turned out to be an adequate trade-off between computational effort and increasing arc length. Parameter estimation was done by least-squares adjustment by the summation of individual arc-wise normal equations to

an overall normal equations system. For each arc, the parameterization was extended by a linear empirical model (bias and drift parameters) in the radial, along-track, and cross-track directions; data analysis was done in the satellite-fixed reference frame.

Gross error detection/elimination was not applied, but we used variance component estimation (VCE) to down-weight orbital sections that contain outliers. The technique weights the individual arcs according to least-squares residuals; i.e., arcs with large residuals have less influence on the parameter estimation compared to arcs with small residuals (cf. Koch and Kusche 2002; Kusche 2003). Every arc entails three variance components, namely one for each coordinate direction. The stochastic model used in the inversion process incorporates the epoch-wise orbit variance-covariance information. In addition, we took empirically derived inter-epoch correlations into account. For this purpose, in an iterative procedure, we derived arc-wise covariance functions from power spectral densities (PSDs) of the least-squares residuals. These covariance functions were used to set up arc-wise variance-covariance matrices.

4.3 Point-wise acceleration approach (PAA)

The PAA balances the gravitational vector with satellite accelerations obtained from numerical differentiation of the kinematic orbit. The method was introduced by Reubelt et al. (2003) and successfully applied to CHAMP (Reubelt 2009) and GOCE (Baur et al. 2012; Reubelt et al. 2013) SST-hl data analysis. Replacing the acceleration term $\mathbf{a}(t)$ in Eq. (1) by the second-order temporal derivative of the satellite position, $\ddot{\mathbf{r}}(t)$, yields the functional model

$$\ddot{\mathbf{r}}(t) - \mathbf{a}_{\mathrm{d}}(t) = \nabla V(t). \tag{3}$$

For numerical differentiation, we applied Gregory–Newton interpolation to successively fit an eighth-order polynomial to nine sampling points (Engeln-Müllges and Reutter 1987). The differentiation scheme is applied along the satellite track, i.e., it can be considered as a moving differentiation filter. The filter moves along the original 1-s orbit, but we chose the sampling point distance to be 5 s (referred to as EDF5, cf. Baur et al. 2012). Double differentiation of the polynomials yields the accelerations $\ddot{\mathbf{r}}(t)$. Due to polynomial oscillations at the interval boundaries, the point under consideration should be in the middle of the differentiation mask; observations affected by the filter warm-up were discarded, implicating a data loss of less than 1 %.

After numerical differentiation, we detected and eliminated gross errors by the comparison of satellite accelerations with forward-evaluated accelerations based on the EGM96 model; the outlier threshold is 4,000 mGal. Both the outdated reference field and the conservative threshold ensure parameter estimation to be independent of a priori gravity field information. Less than 0.01 % of the data was classified as gross errors. In addition to gross error elimination, we applied VCE for the relative weighting of orbital arcs (cf. Sect. 4.2).

Parameter estimation was done by least-squares adjustment in terms of arc-wise normal equation system assembly with an arc length of 15 min. Constant empirical accelerations in each direction have been considered once for every ten successive arcs (i.e., once for every 150 min). This "best choice" for both the arc length and the setup of empirical parameters was found by trial and error (cf. Baur et al. 2012; Reubelt et al. 2013). Straightforward error propagation was performed starting from the inner-epoch orbit variance-covariance information. The data analysis was done in the satellite-fixed reference frame.

4.4 Averaged acceleration approach (AAA)

The AAA has been successfully applied in the compilation of a number of Earth gravity field models, including the DEOS_CHAMP-01C_70 solution derived from CHAMP data (Ditmar et al. 2006) and the DGM-1S model based on data acquired by GRACE and GOCE (Hashemi Farahani et al. 2013). The functional model of the AAA is described in Ditmar and van Eck van der Sluijs (2004) and shows similarities to the one of the PAA (cf. Sect. 4.3). However, instead of fitting an eighth-order polynomial to nine sampling points, the satellite accelerations are derived by the 3-point double-differentiation scheme

$$\bar{\ddot{\mathbf{r}}}(t) = \frac{\mathbf{r}(t-\Delta t) - 2\mathbf{r}(t) + \mathbf{r}(t+\Delta t)}{(\Delta t)^2}, \tag{4}$$

with Δt denoting the sampling interval. In principle, these accelerations should be interpreted as average accelerations with weight $w(s)$ in the differentiation interval, according to

$$\bar{\ddot{\mathbf{r}}}(t) = \int_{-\Delta t}^{\Delta t} w(s)\, \ddot{\mathbf{r}}(t+s)\, \mathrm{d}s; \quad w(s) = \frac{\Delta t - |s|}{(\Delta t)^2}. \tag{5}$$

However, as has been suggested by Ditmar and van Eck van der Sluijs (2004), for densely sampled orbits as in the case of GOCE, the averaging effect can be neglected.

As mentioned earlier (see Sect. 3), our AAA implementation does not make use of the provided variance-covariance information but the stochastic model was set up empirically. The strategy is described in Ditmar et al. (2007); it is based on an auto-regressive (AR) model to represent inter-epoch correlations and an inner-epoch diagonal weight matrix (i.e., epoch-wise correlations between the three components of $\ddot{\mathbf{r}}(t)$ were not taken into account). The analysis was done in the satellite-fixed reference frame with variable arc lengths according to the occurrence of data gaps.

The gravity field and the stochastic model were determined simultaneously in an iterative procedure. In the first

iteration, an initial gravity field solution up to d/o 20 was computed under the assumption of white noise (no temporal correlations, unit weights). From the corresponding least-squares residuals, we derived the initial AR model parameters and updated the entries of the diagonal weight matrix. The AR model was determined by first calculating the PSDs of the residuals by Welch's method (Welch 1967). Next, the PSDs were transformed into auto-covariances, from which the AR model coefficients were calculated by Levinson–Durbin recursion (Durbin 1960). The elements of the diagonal weight matrix were calculated by taking the variance inside a moving 21-point window (found by trial and error) of the time-decorrelated residuals. In the following iterations, the maximum spectral resolution was successively increased to d/o 130 while updating the stochastic model from iteration to iteration. The procedure stopped once "visual inspection" revealed no further changes of the stochastic model and gravity field solution (about ten iterations in total). Tests on the co-estimation of empirical parameters showed that their incorporation does not improve the gravity field estimates; hence, we did not consider them.

4.5 Energy balance approach (EBA)

The EBA (also known as energy integral approach) makes use of the principle of energy conservation (O'Keefe 1957). The method was successfully applied to infer gravity fields from various LEO missions; examples include the CHAMP (Badura et al. 2006) and GOCE satellites. The EBA was considered for the compilation of the first three releases of the GOCE-TIM gravity field models (Pail et al. 2011); details about the implementation that underlies the EBA solutions presented in this study can be found in Badura (2006). The principle of energy conservation implies the sum of potential energy (E_p), kinetic energy (E_k), and dissipation energy (E_d) to be constant, $E_\mathrm{p}+E_\mathrm{k}+E_\mathrm{d}=\text{const}$. Further, kinetic energy relates to the geopotential $V(t)$ and the motion of a satellite according to

$$V(t) = E_\mathrm{k} + C = \frac{1}{2}\|\dot{\mathbf{r}}(t)\|^2 + C. \tag{6}$$

Therein, $\dot{\mathbf{r}}(t)$ is the satellite velocity and C denotes the constant of integration.

According to Eq. (6), the idea behind the EBA is to estimate the gravity field parameters (together with the constant of integration) from satellite velocity magnitudes. The GOCE velocities were derived from the 1-s kinematic orbit by numerical differentiation (this processing step is akin to the computation of satellite accelerations for the PAA, cf. Sect. 4.4). We used a Taylor–MacLaurin differentiation scheme (Goiginger and Pail 2006), which is based on the solution of an over-determined system of equations.

Although Eq. (6) constitutes a linear functional model, we estimated the gravity field parameters by iterative least-squares adjustment to detect and eliminate gross errors. Within the subsequent iterations, the standard deviation of the residual energy time series (computed energy based on the model parameters minus "observed" energy) was used for outlier detection/elimination according to a $5\,\sigma$-threshold criterion. The iterative process stopped when all residuals passed the outlier test.

Depending on the occurrence of data gaps, we split the kinematic orbit into arcs with minimum and maximum arc length of 92 and 5,500 points, respectively. For each arc, the parameterization was extended by a linear drift term and a quadratic term (in addition, the constant of integration C may be considered as a constant empirical parameter). The total orbit variance-covariance information was used to perform rigorous error propagation within each individual processing step (cf. Goiginger and Pail 2010).

5 Performance measures

All gravity fields used in this study are given in terms of an expansion in spherical harmonics (cf. Heiskanen and Moritz 1967). The gravity field coefficients are denoted here as $v_{nm} = \{c_{nm}, s_{nm}\}$; n and m indicate the degree and order of the spherical harmonic series, respectively. Performance measures in the spectral domain include formal errors $\sigma_{v_{nm}}$ and empirical errors $\varepsilon_{v_{nm}}$. The empirical errors are relative to the ITG-Grace2010s model (Mayer-Gürr et al. 2010), one of the state-of-the-art GRACE-only gravity field solutions:

$$\varepsilon_{v_{nm}} = \left\| \frac{v_{nm}^{\mathrm{grace}} - v_{nm}}{v_{nm}^{\mathrm{grace}}} \right\|. \tag{7}$$

Displayed degree-error root mean square (DE-RMS) values (in terms of geoid heights) are according to

$$\text{DE-RMS}_n = R\sqrt{\frac{1}{2n+1}\sum\nolimits_{m=0}^{n}[(c_{nm}^{\mathrm{grace}} - c_{nm})^2 + (s_{nm}^{\mathrm{grace}} - s_{nm})^2]}, \tag{8}$$

with reference radius $R = 6{,}378{,}137$ m. To account for the polar gap problem, for some representations, an additional measure of model accuracy is used in which orders $m \le m_n = |0.5\pi - I|\, n$ (with orbit inclination I in radians) were omitted (Van Gelderen and Koop 1997). Cumulative geoid height errors σ_N have been computed by

$$\sigma_\mathrm{N} = \sqrt{\sum\nolimits_{n=2}^{n_\mathrm{max}}(2n+1)\text{DE-RMS}_n^2}. \tag{9}$$

If formal errors are considered, the terms $(c_{nm}^{\mathrm{grace}} - c_{nm})$ and $(s_{nm}^{\mathrm{grace}} - s_{nm})$ in Eq. (8) were replaced by $\sigma_{c_{nm}}$ and $\sigma_{s_{nm}}$, respectively. In the spatial domain, we evaluated geoid height

differences with respect to the ITG-Grace2010s model (starting at d/o 3); Gaussian smoothing with a radius of 500 km was applied to suppress high-frequency noise.

Finally, we investigated satellite laser ranging (SLR) residuals from dynamic precise orbit determination (POD) of geodetic satellites. These residuals were obtained as the difference between observed ranges and computed ranges. The latter are the distances between ground stations and the adjusted orbit using SLR data. As dynamic POD depends on the underlying force models, SLR residuals are a measure for the quality of the adopted gravity field information (cf. Sośnica et al. 2012). POD is particularly suited to evaluate the quality at the longer wavelengths, which is due to the strong attenuation of the gravity signal with altitude. We analyzed ranges (SLR normal point data) to the LAGEOS-1 and Starlette satellites. These geodetic satellites have an orbital altitude of about 5,800 and 800 km, respectively. As a consequence, orbit perturbations of LAGEOS-1 are only sensitive to the very long wavelengths (we considered gravity field coefficients up to d/o 20), whereas medium-wavelength information should be considered for Starlette (coefficients up to d/o 100 were taken into account). We accomplished POD for the year 2012 in monthly continuous arcs under consideration of the GOCE-GPS gravity field models derived from the different analysis approaches. The estimated parameters are state vectors (1/arc), station coordinates (1 set/station and arc), drag coefficients (1/day), constant empirical accelerations in each direction (1/day) and measurement biases (1/station and arc). The same set of SLR ranges has been used for every POD computation; the total number of normal points is 59,061 and 71,370 for LAGEOS-1 and Starlette, respectively.

6 Results

6.1 Formal errors and empirical errors

Figure 1 displays formal errors (left column) and empirical errors (right column) of the estimated spherical harmonic coefficients. The patterns are in very good agreement for the CMA, SAA, PAA, and AAA. This holds true for the same type of errors (formal or empirical) for the different approaches as well as for the formal and empirical errors of each approach. The (near-)zonal and high-degree coefficients show large uncertainties. The former is due to the polar data gap, whereas the latter can be attributed to high-frequency noise and spectral aliasing caused by the limited resolution of the gravity field models. Except for EBA, the quality of the (near-)sectorial coefficients is superior to the quality of the tesseral coefficients of like degree, because sectorial terms generate long-wavelength perturbations along a polar orbit (Beutler et al. 2010b). As far as the EBA solution is concerned, the (near-)sectorial and tesseral coefficients of like degree show comparable accuracies. We attribute this distinct feature to the fact that—in contrast to all other approaches—the method considers scalar-valued information (satellite velocity magnitudes, cf. Sect. 4.5); the usage of 1D-observables opposed to 3D-observables impacts the gravity field solution, but also the associated covariance structure.

The EBA estimate seems to be less affected by the polar data gap compared to the other solutions. However, this first assessment does not go far enough. We confirm the finding by Sneeuw and van Gelderen (1997), who found that the impact of the polar gap significantly depends on the maximum spectral resolution $n_{\max}$ of the recovered gravity field parameters (see also Jäggi et al. 2011b). The influence of the polar gap increases with increasing $n_{\max}$, i.e., the higher the maximum resolution, the more low-order coefficients become distorted (not shown here). For this reason, the polar gap problem (poor quality of the (near-)zonal coefficients) is less pronounced for the EBA solution ($n_{\max} = 100$) opposed to the other gravity fields ($n_{\max} = 130$).

The findings from the inspection of the formal errors and empirical errors are underlined by the DE-RMS representation of the solutions (Fig. 2). In addition to GOCE-GPS gravity fields, Fig. 2 contains the GOCE-TIM models for the respective analysis periods. From kinematic GOCE orbit analysis, the gravity field can be recovered (signal-to-noise ratio ≥ 1) up to d/o $\approx$110 and $\approx$120 for the R1 period and R2 period, respectively. CMA, SAA, PAA, and AAA show comparable performance. The EBA solutions are worse by a factor of about $\sqrt{3}$; this issue is addressed in more detail in Sect. 7. The EBA solutions displayed in Fig. 2 have been considered for the first two releases of the GOCE-TIM models; for this reason, the respective graphs coincide in the long-wavelength spectra (up to d/o $\approx$20). With increasing spherical harmonic degree, the impact of satellite gravity gradiometry on the GOCE-TIM estimates steadily increases; the SST-hl contribution to the recovered geopotential parameters decreases accordingly. [Side remark: for the EBA, besides a scaling factor the empirical and the formal error curves are in very good agreement over a vast part of the spectrum. Thus, the suspicion arises that the formal errors are improperly scaled. This might indeed be true, but could not be confirmed from the available information on the EBA solutions. We decided to refrain from any "artificial" scaling].

As has been emphasized earlier, the apparently lower impact of the polar data gap on the EBA solution (Fig. 2, bottom panel) can be explained with differences of the maximum spectral resolution ($n_{\max} = 100$ versus $n_{\max} = 130$). The polar gap problem is even less pronounced for the GOCE-TIM models; this is because constraints in terms of Kaula regularization were applied to (near-)zonal coefficients (Pail et al. 2011). On the other hand, the CMA and SAA seem to be strongely affected by the polar data gap com-

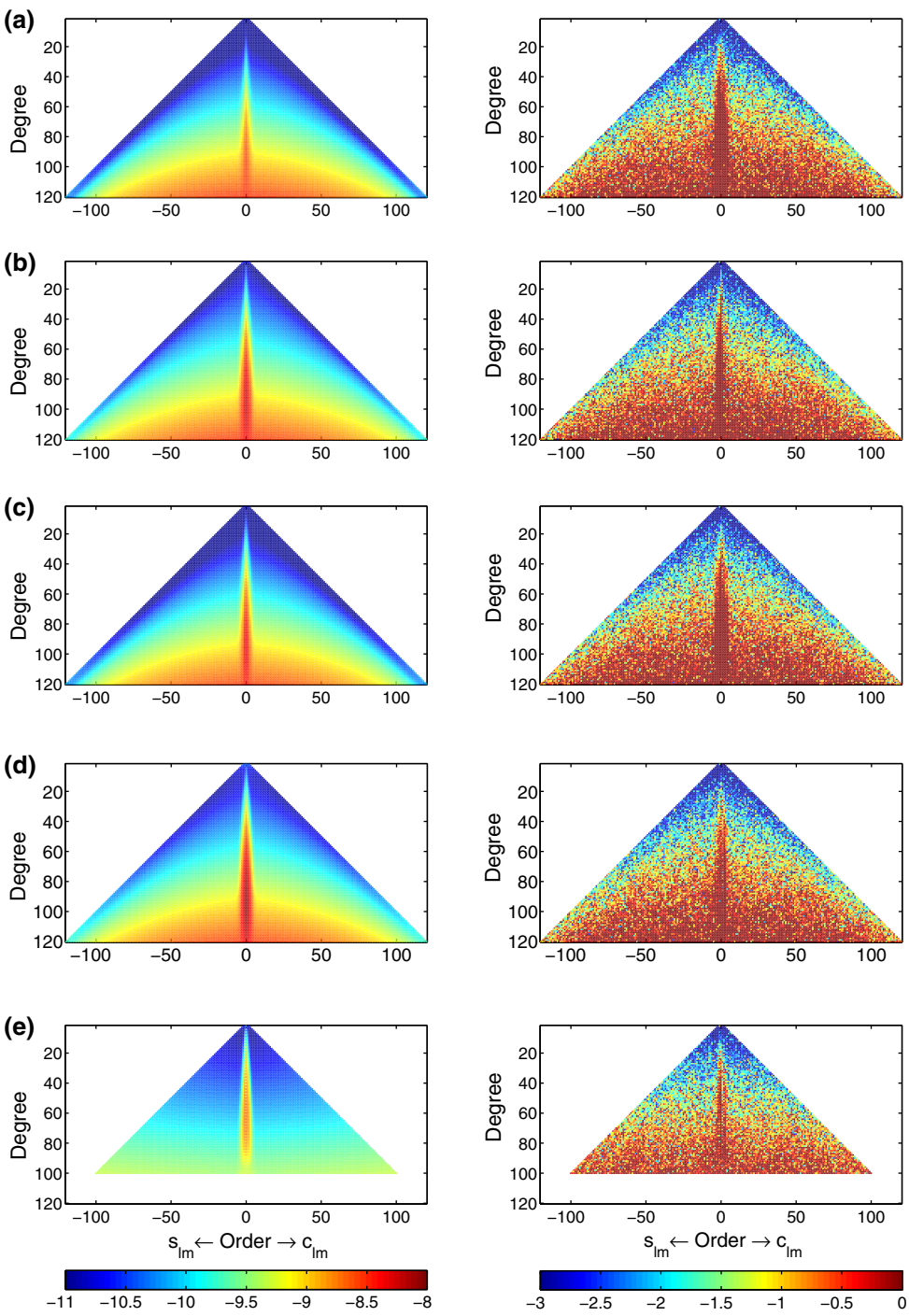

Fig. 1 Formal errors (*left column*) and empirical errors w.r.t. ITG-Grace2010s (*right column*) of spherical harmonic coefficients (log 10 representation). Results based on GOCE kinematic orbit analysis from the R1 period using the **a** CMA, **b** SAA, **c** PAA, **d** AAA, and **e** EBA

pared to the PAA and AAA. The occurrence of the zig-zag behavior for some of the DE-RMS curves is not yet fully understood.

6.2 Geoid height differences and cumulative geoid height errors

Figure 3 presents the spatial-domain representation of the GOCE-GPS gravity fields in terms of geoid height differences. The CMA, SAA, PAA, and AAA patterns are in good agreement. The most striking feature is the near-equatorial "band", correlating with the magnetic equator of the Earth; it is more pronounced in the solutions over the R2 period than those over the R1 period. We attribute this feature to systematic orbit errors around the geomagnetic equator; the systematic errors get more pronounced from year to year due to the increasing solar activity during the mission duration. Compared to the other solutions, the EBA patterns are much

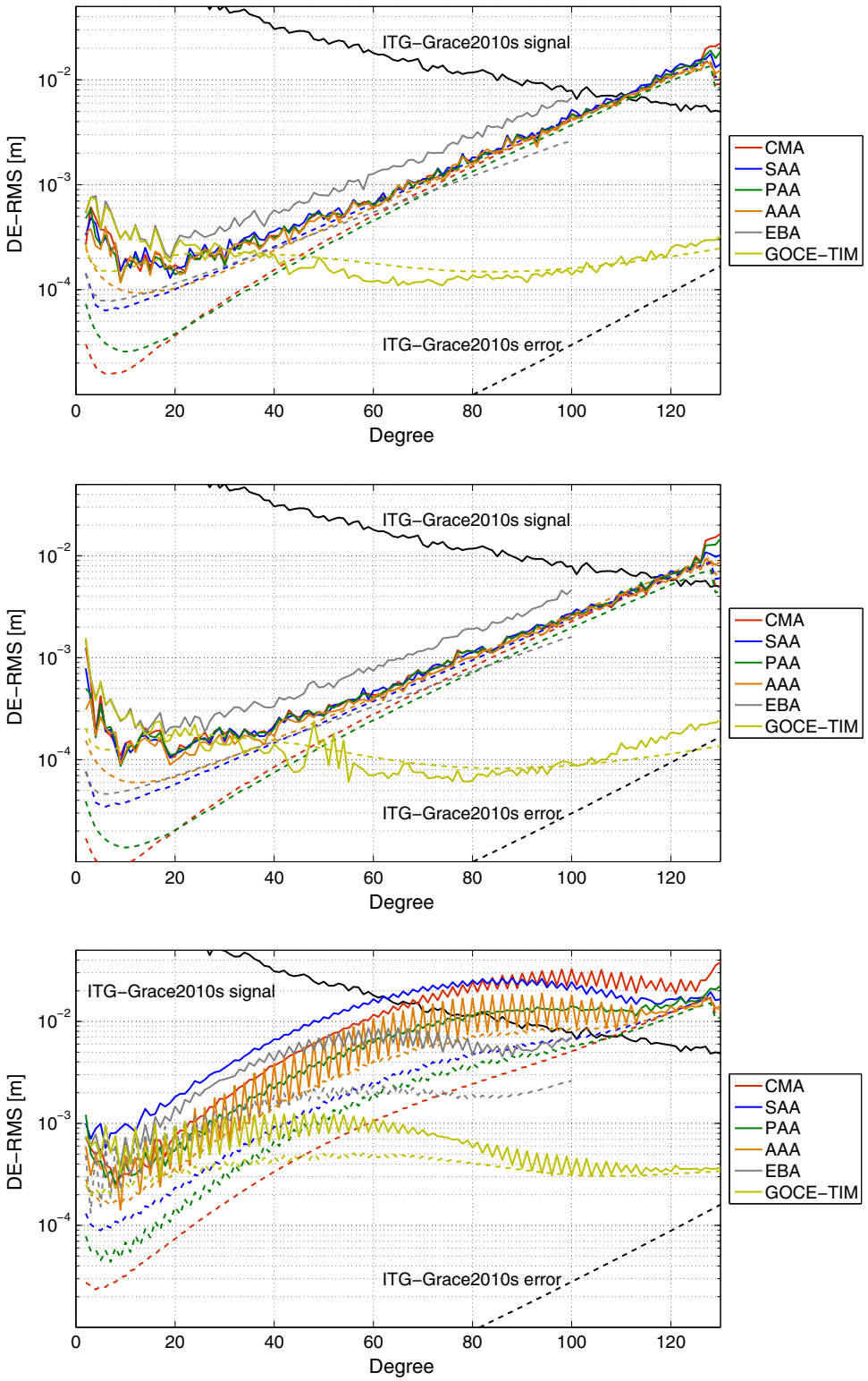

Fig. 2 Results for the R1 period (*top and bottom*) and the R2 period (*middle*). *Black solid graph* ITG-Grace2010s signal; *solid color graphs* DE-RMS of recovered spherical harmonic coefficients; *dashed graphs* formal errors. *Top and middle* orders $m \leq m_n$ omitted; *bottom* all orders considered

noisier; the geomagnetic equator is not visible for the R1 period, but appears for R2.

Figure 4 shows cumulative geoid height errors for the R1 period. The accuracy of the GOCE-GPS models is about 18 cm at d/o 100 (corresponding to a spatial resolution of ≈200 km half wavelength), cf. Table 2; for R2, the accuracy increases to about 11 cm. Most of the values in the columns 3 and 5 are considerably smaller than the values in the columns 2 and 4, which is due to over-optimistic formal errors (cf. Fig. 2). This holds particularly true for the

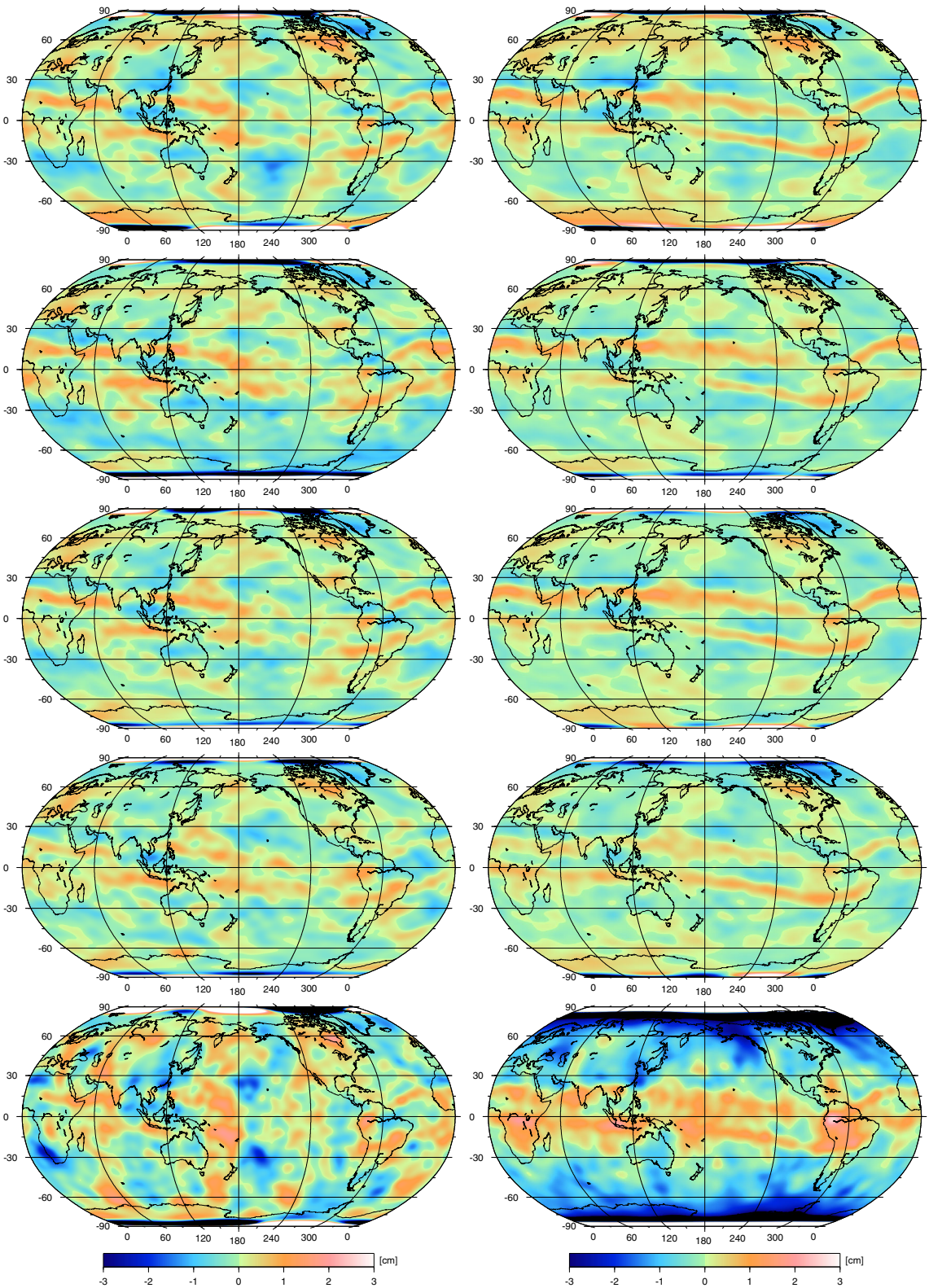

Fig. 3 Geoid height differences w.r.t. to ITG-Grace2010s (d/o 3–60). Results based on GOCE kinematic orbit analysis for the R1 period (*left column*) and the R2 period (*right column*); Gaussian smoothing with a radius of 500 km applied. From *top to bottom* CMA, SAA, PAA, AAA, EBA

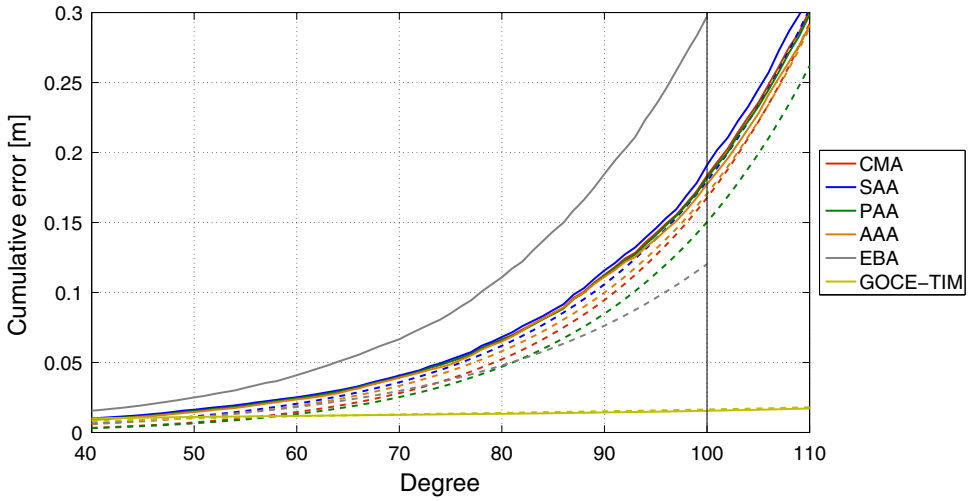

Fig. 4 Cumulative geoid height errors of GOCE-GPS gravity fields based on orbit analysis for the R1 period. *Solid graphs* derived from empirical errors w.r.t. ITG-Grace2010s; *dashed graphs* derived from formal errors. Orders $m \leq m_n$ omitted

Table 2 Cumulative geoid height errors (cm) at d/o 100

Approach	R1 period		R2 period	
	Empirical	Formal	Empirical	Formal
CMA	18.3	16.8	11.3	9.2
SAA	19.1	18.0	11.6	10.2
PAA	18.2	15.0	11.3	8.0
AAA	17.7	17.1	10.4	11.1
EBA	29.7	12.0	19.1	7.3
GOCE-TIM	1.6	1.6	1.0	1.0

Orders $m \leq m_n$ omitted, cf. Sect. 5

EBA solutions. According to Fig. 2, from d/o ≈80−100, the EBA formal errors are smallest compared to the other GOCE-GPS estimates. Due to the slope of the degree variances, the cumulative errors are dominated by these high degrees; this explains the course of the (formal) errors curves in Fig. 4 and the numerical values in Table 2. The empirical and formal cumulative geoid height errors match for the GOCE-TIM releases; owing to satellite gravity gradiometry, the numerical values are much smaller compared to the other models.

6.3 SLR residuals

The RMS of SLR residuals from POD of the LAGEOS-1 satellite is shown in Fig. 5. The top panel reveals considerable variation for the different GOCE-GPS gravity fields. The main reason for this behavior could be traced back to the recovery of the c_{20} coefficients; after replacement of the c_{20} value of all our GOCE-GPS solutions with a reference value (here the value of the GOCE-DIR release-4 gravity field model was used), most of the variation vanishes (Fig. 5, panel (b)). The remaining variation is due to the polar gap problem. As has been concluded in Sect. 6.1 (especially Fig. 2, bottom panel), the SAA solutions are mostly affected by the lack of data in the polar regions. This characteristic is supported by the SLR residuals.

To demonstrate the sensitivity of the SLR residuals against the polar gap problem, Fig. 5 (panel (d)) presents the results after the replacement of the orders $m \leq m_n$ by coefficients from the GOCE-DIR release-4 model (Bruinsma et al. 2013); this model was derived from GOCE, GRACE and SLR data in combination with tailored (spherical cap) regularization, and hence circumvents the problem of a poor estimation of the (near-)zonal coefficients. After replacement, very similar results were obtained for all solutions. Indeed, the sensitivity against the polar data gap can be attributed to solely the zonal coefficients (Fig. 5, panel (c)).

The results over the R1 period for LAGEOS-1 also hold for Starlette, as well as for SLR residuals from GOCE-GPS solutions derived for the R2 period (Table 3). As far as the magnitude of the tracking residuals is concerned, it should be emphasized that it has not been our intention to minimize absolute values, but the focus is on the relative performance of the different gravity fields; nevertheless, annual RMS values of about 2.3 and 13.1 cm for LAGEOS-1 and Starlette, respectively, demonstrate adequate parameterization for the POD of the considered geodetic satellites.

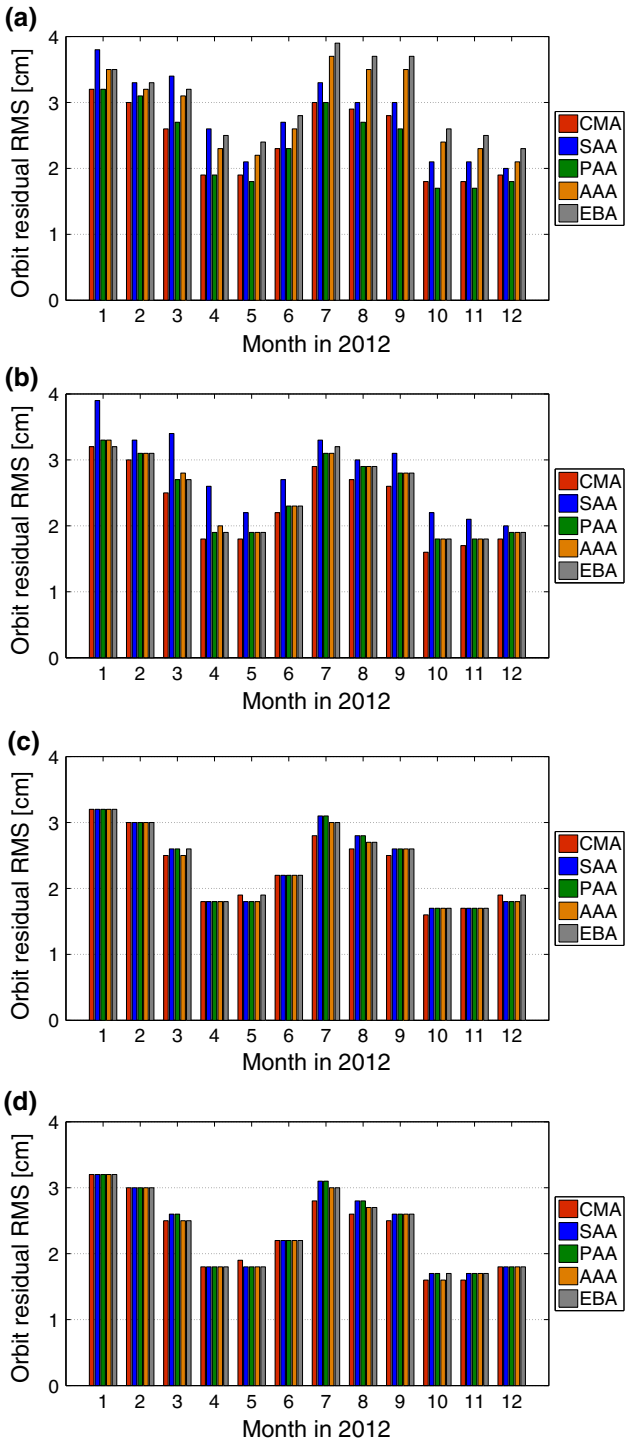

Fig. 5 SLR residuals (observed minus computed) of LAGEOS-1 adopting different gravity fields for precise orbit determination ($n_{\max} = 20$, R1 period). **a** original solutions, **b** c_{20} coefficients replaced by GOCE-DIR values, **c** zonal coefficients replaced, **d** orders $m \leq m_n$ replaced

Table 3 SLR residuals (cm) for LAGEOS 1 ($n_{\max} = 20$) and Starlette ($n_{\max} = 100$)

Approach	LAGEOS 1				Starlette			
			c_{n0} replaced				c_{n0} replaced	
	R1	R2	R1	R2	R1	R2	R1	R2
CMA	2.4	2.3	2.3	2.3	16.2	14.2	13.1	13.2
SAA	2.8	2.3	2.4	2.4	17.5	14.3	13.2	13.2
PAA	2.4	2.4	2.4	2.4	14.6	14.9	13.2	13.2
AAA	2.9	3.2	2.3	2.3	20.2	29.6	13.0	13.0
EBA	3.0	8.1	2.4	2.4	28.3	26.2	13.1	13.1

RMS values for the year 2012

7 Discussion

Based on various performance measures, we found GOCE-GPS gravity field solutions derived from the application of the CMA, the SAA, the PAA, and the AAA to have comparable quality. Without any attempt to "rank" the solutions investigated in this study (the estimates are very close to each other), from the cumulative geoid height errors in Table 2, it appears that the AAA solutions are slightly superior to the other estimates. This is also supported by the DE-RMS curves in Fig. 2 (top and middle panels). In the presence of the polar gap, the AAA and PAA solutions are equivalent; they perform slightly better than the CMA and SAA gravity fields.

As far as the SLR residuals are concerned, all approaches yield equivalent results if the (near-)zonal coefficients are replaced by reference values. This is because of the sensitivity of SLR towards gravity field constituents. The sensitivity is largest for the low-degree coefficients (mainly c_{20}, followed by some more zonal coefficients). As a consequence, as far as the (relative) performance of our GOCE-GPS gravity fields is concerned, SLR residuals are mainly a measure to evaluate the impact of the polar gap problem on the individual solutions. Without replacement, the CMA and PAA slightly outperform the SAA, whereas the EBA and AAA solutions show noticeably larger residuals.

The EBA, on the other hand, shows systematic shortcomings (Fig. 6). As has been proven from theoretical assessment and earlier numerical studies (e.g., Ditmar and van Eck van der Sluijs 2004; Mayer-Gürr et al. 2005b; Reubelt et al. 2012), the EBA is inferior to the other approaches by a factor of about $\sqrt{3}$. This inferiority can be explained from a statistical point of view. Vector-valued velocity is transferred into scalar-valued energy (cf. Eq. (6)), implying a loss of

redundancy by the factor of 3, and hence a degradation of the solution by the factor of $\sqrt{3}$.

It has to be emphasized that data processing consistency is of utmost importance to fairly evaluate the performance of different inference approaches against each other. Otherwise, possible differences between the estimates may be misinterpreted. As an example, Fig. 7 sheds light on the incorporation/neglect of the (residual) non-gravitational accelerations in the analysis. The satellite surface accelerations impact the long-wavelength spherical harmonic coefficients up to d/o ≈25, but mainly distort the estimation of the degree-2 gravity field parameters.

An open issue common to all GOCE-GPS gravity field solutions is the misfit between the formal and the "true" errors. Especially in the long-wavelength part, the formal errors are over-optimistic; for CMA and PAA, they deviate up to one order of magnitude from the "true" errors (cf. Fig. 2). The discrepancies hint to shortcomings of the stochastic model (Reubelt et al. 2013). The provided variance-covariance information just reflects the mathematical propagation of random carrier phase errors into the kinematic positions when simultaneously estimating carrier phase ambiguities and epoch-wise receiver clock corrections in addition to the orbit. Any types of unmodeled systematic errors are not reflected by the SST_PCV_2 product (Jäggi et al. 2011a). The incorporation of empirical covariance information for inter-epoch correlations (as considered for the SAA and AAA solutions) yields improved agreement between the formal and the true errors.

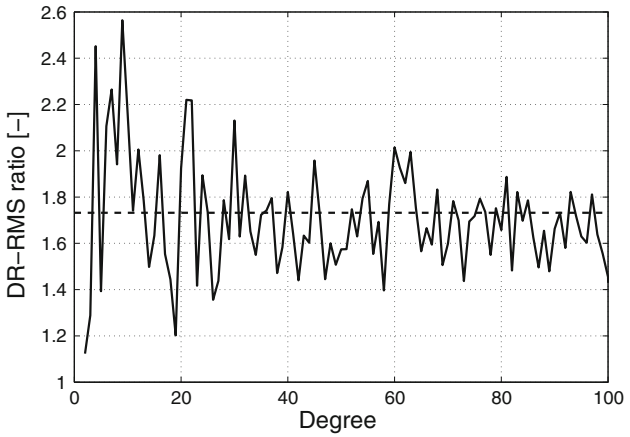

Fig. 6 *Solid graph* DE-RMS ratios between the PAA solution and the EBA solution (R1 period); *dashed line* displays the $\sqrt{3}$ level

8 Conclusions

Disregarding energy balance, we conclude that the gravity field recovery approaches considered in this study have compatible performance; the solutions based on the energy conservation principle are inferior due to inherent shortcomings. This overall assessment can be drawn due to a large degree of consistency in the data processing. On the other hand, it should be noted that each methodology requires individual adaptation, often accompanied by trial-and-error procedures. This holds particularly true for the setup of empirical parameters, which allow "steering" of the gravity field solution performance to a certain extent. From the analysis of kinematic GOCE orbits over the periods R1 (November 1, 2009

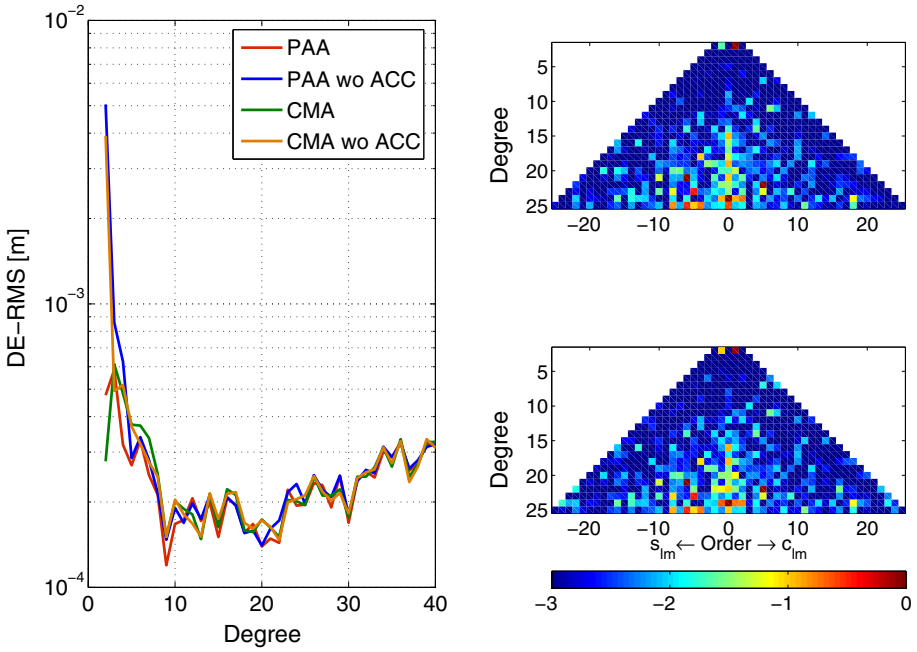

Fig. 7 Impact of non-gravitational accelerations (R1 period). *Left* DE-RMS of recovered spherical harmonic coefficients (orders $m \leq m_n$ omitted); for solutions labeled 'wo ACC', non-gravitational accelerations were neglected. *Right* empirical errors w.r.t. ITG-Grace2010s; *top* non-gravitational accelerations considered, *bottom* non-gravitational accelerations neglected

to January 11, 2010) and R2 (November 1, 2009 to July 5, 2010), we found the cumulative geoid height errors at d/o 100 to about 18 and 11 cm, respectively.

We want to emphasize that the investigations presented in this paper must not solely be seen in the context of GOCE gravity field determination. With regard to a possible gap between the GRACE and GRACE follow-on satellite missions, the exploitation of SST-hl data of low Earth orbiting spacecraft—such as Swarm—might constitute a valuable bridging technique for very long-wavelength time-variable gravity field recovery (especially when the satellites are equipped with accelerometers to measure the influence of surface forces). The potential of kinematic orbit analysis for this purpose has recently been demonstrated (Weigelt et al. 2013; Baur 2013). Although these first results are very promising, we want to emphasize that it is very unlikely that SST-hl will ever reach the GRACE performance.

Acknowledgments Precise orbit determination of SLR satellites was accomplished with the software package GEODYN, kindly provided by the NASA Goddard Space Flight Center. Support by Mattias Roth (orbit data preparation) for the PAA results is acknowledged. Furthermore, we thank Roland Pail for implementational details underlying the energy balance approach solutions, as well as Pavel Ditmar and Hassan Hashemi Farahani for discussions concerning the averaged acceleration approach. Last but not least, we are grateful for the comments and suggestions by three anonymous reviewers.

References

Badura T (2006) Gravity field analysis from satellite orbit information applying the energy integral approach. PhD Thesis, Graz University of Technology, Austria

Badura T, Sakulin C, Gruber C, Klostius R (2006) Derivation of the CHAMP-only global gravity field model TUG-CHAMP04 applying the energy integral approach. Stud Geophys Geod 50:59–74. doi:10.1007/s11200-006-0002-3

Baur O (2013) Greenland mass variation from time-variable gravity in the absence of GRACE. Geophys Res Lett 40:4289–4293. doi:10.1002/grl.50881

Baur O, Reubelt T, Weigelt M, Roth M, Sneeuw N (2012) GOCE orbit analysis: long-wavelength gravity field determination using the acceleration approach. Adv Space Res 50:385–396. doi:10.1016/j.asr.2012.04.022

Beutler G, Jäggi A, Mervart L, Meyer U (2010a) The celestial mechanics approach: theoretical foundations. J Geod 84:605–624. doi:10.1007/s00190-010-0401-7

Beutler G, Jäggi A, Mervart L, Meyer U (2010b) The celestial mechanics approach: application to data of the GRACE mission. J Geod 84:661–681. doi:10.1007/s00190-010-0402-6

Bock H, Jäggi A, Meyer U, Visser P, van den IJssel J, van Helleputte T, Heinze M, Hugentobler U (2011) GPS-derived orbits for the GOCE satellite. J Geod 85:807–818. doi:10.1007/s00190-011-0484-9

Bruinsma SL, Förste C, Abrikosov O, Marty J-C, Rio M-H, Mulet S, Bonvalot S (2013) The new ESA satellite-only gravity field model via the direct approach. Geophys Res Lett 40:3607–3612. doi:10.1002/grl.50716

Ditmar P, van Eck van der Sluijs A (2004) A technique for modeling the Earth's gravity field on the basis of satellite accelerations. J Geod 78:12–33. doi:10.1007/s00190-003-0362-1

Ditmar P, Kuznetsov V, van Eck van der Sluijs AA, Schrama E, Klees R (2006) DEOS_CHAMP-01C_70: a model of the Earth's gravity field computed from accelerations of the CHAMP satellite. J Geod 79:586–601. doi:10.1007/s00190-005-0008-6

Ditmar P, Klees R, Liu X (2007) Frequency-dependent data weighting in global gravity field modeling from satellite data contaminated by non-stationary noise. J Geod 81:81–96. doi:10.1007/s00190-006-0074-4

Drinkwater MR, Haagmans R, Muzi D, Popescu A, Floberghagen R, Kern M, Fehringer M (2007) The GOCE gravity mission: ESA's first core Earth explorer. In: Proceedings of 3rd international GOCE user workshop, Frascati, Italy, ESA SP-627, pp 1–8

Durbin J (1960) The fitting of time series models. Rev Int Stat Inst 28:233–244

EGG-C (2006) GOCE L1b products user handbook. GOCE-GSEG-EOPG-TN-06-0137, Issue 1.1

EGG-C (2010) GOCE Level 2 product data handbook. GO-MA-HPF-GS-0110, Issue 4.3

Engeln-Müllges G, Reutter F (1987) Numerische Mathematik für Ingenieure. BI Wissenschaftsverlag, Zurich (in German)

ESA (1999) The four candidate Earth Explorer Core Missions-Gravity Field and Steady-State Ocean Circulation Mission. ESA SP-1233

ESA (2011) GOCE Newsletter. Issue 2, Rev. 1. Web access. https://earth.esa.int/web/guest/-/goce-newsletters-7007

Flechtner F, Dahle C, Neumayer KH, König R, Förste C (2010) The release 04 CHAMP and GRACE EIGEN gravity field models. In: Flechtner F et al. (eds) System earth via geodetic-geophysical space techniques. Springer, Berlin, pp 41–58. doi:10.1007/978-3-642-10228-8_4

Gerlach C, Sneeuw N, Visser P, Švehla D (2003) CHAMP gravity field recovery using the energy balance approach. Adv Geosci 1:73–80. doi:10.5194/adgeo-1-73-2003

Goiginger H, Pail R (2006) Investigation of velocities derived from satellite positions in the framework of the energy integral approach. In: Proceedings 3rd GOCE user workshop, Frascati, Italy, ESA SP-627, pp 319–324

Goiginger H, Pail R (2010) Covariance propagation of latitude-dependent orbit errors within the energy integral approach. In: Mertikas SP (ed) IAG symposium on gravity, geoid and earth observation, vol 135. Springer, Berlin, pp 155–161. doi:10.1007/978-3-642-10634-7_21

Han S-C, Jekeli C, Shum CK (2002) Efficient gravity field recovery using in situ disturbing potential observables from CHAMP. Geophys Res Lett 29:1789. doi:10.1029/2002GL015180

Hashemi Farahani H, Ditmar P, Klees R, Liu X, Zhao Q, Guo J (2013) The static gravity field model DGM-1S from GRACE and GOCE data: computation, validation and an analysis of GOCE mission's added value. J Geod 87:843–867. doi:10.1007/s00190-013-0650-3

Heiskanen WA, Moritz H (1967) Physical geodesy. WH Freeman and Company, San Francisco

Jäggi A, Hugentobler U, Beutler G (2006) Pseudo-stochastic orbit modeling techniques for low-Earth orbiters. J Geod 80:47–60. doi:10.1007/s00190-006-0029-9

Jäggi A, Beutler G, Prange L, Dach R, Mervart L (2009) Assessment of GPS-only observables for gravity field recovery from GRACE. In: Sideris M (ed) IAG symposium on observing our changing earth, vol 133. Springer, Berlin, pp 113–123. doi:10.1007/978-3-540-85426-5_14

Jäggi A, Prange L, Hugentobler U (2011a) Impact of covariance information of kinematic positions on orbit reconstruction and gravity field recovery. Adv Space Res 47:1472–1479. doi:10.1016/j.asr.2010.12.009

Jäggi A, Bock H, Prange L, Meyer U, Beutler G (2011b) GPS-only gravity field recovery with GOCE, CHAMP, and GRACE. Adv Space Res 47:1020–1028. doi:10.1016/j.asr.2010.11.008

Jäggi A, Beutler G, Meyer U, Prange L, Dach R, Mervart L (2012) AIUB-GRACE02S—status of GRACE gravity field recovery using the celestial mechanics approach. In: Kenyon S, Pacino MC, Marti U (eds) IAG symposium on geodesy for planet earth, vol 136. Springer, Berlin, pp 161–169. doi:10.1007/978-3-642-20338-1_20

Koch K-R, Kusche J (2002) Regularization of geopotential determination from satellite data by variance components. J Geod 76:259–268. doi:10.1007/s00190-002-0245-x

Kusche J (2003) A Monte-Carlo technique for weight estimation in satellite geodesy. J Geod 76:641–652. doi:10.1007/s00190-002-0302-5

Lemoine FG, Kenyon SC, Factor JK, Trimmer RG, Pavlis NK, Chinn DS, Cox CM, Klosko SM, Luthcke SB, Torrence MH, Wang YM, Williamson RG, Pavlis EC, Rapp RH, Olson TR (1998) The development of the joint NASA GSFC and NIMA geopotential model EGM96. NASA Goddard Space Flight Center, Greenbelt

Mayer-Gürr T (2006) Gravitationsfeldbestimmung aus der Analyse kurzer Bahnbögen am Beispiel der Satellitenmissionen CHAMP und GRACE. PhD Thesis, Rheinische Friedrich-Wilhelms-Universität zu Bonn (in German)

Mayer-Gürr T, Ilk KH, Eicker A, Feuchtinger M (2005a) ITG-CHAMP01: a CHAMP gravity field model from short kinematic arcs over a one-year observation period. J Geod 78:462–480. doi:10.1007/s00190-004-0413-2

Mayer-Gürr T, Feuchtinger M, Kusche J (2005b) A comparison of various procedures for global gravity field recovery from CHAMP orbits. In: Reigber C, et al. (eds) Earth observation with CHAMP–results from three years in orbit. Springer, Berlin, pp 151–156. doi:10.1007/3-540-26800-6_24

Mayer-Gürr T, Kurtenbach E, Eicker A (2010) The satellite-only gravity field model ITG-Grace2010s. http://www.igg.uni-bonn.de/apmg/index.php?id=itg-grace2010

Meissl P (1971) On the linearization of the geodetic boundary value problem. Report 151, Department of Geodetic Science and Surveying, Ohio State University Columbus

O'Keefe JA (1957) An application of Jacobi's integral to the motion of an earth satellite. Astron J 62:265–266. doi:10.1086/107530

Pail R, Bruinsma S, Migliaccio F, Förste C, Goiginger H, Schuh W-D, Höck E, Reguzzoni M, Brockmann JM, Abrikosov O, Veicherts M, Fecher T, Mayrhofer R, Krasbutter I, Sansò F, Tscherning CC (2011) First GOCE gravity field models derived by three different approaches. J Geod 85:819–843. doi:10.1007/s00190-011-0467-x

Prange L (2011) Global gravity field determination using the GPS measurements made onboard the low earth orbiting satellite CHAMP. Geodätisch-geophysikalische Arbeiten in der Schweiz, 81

Prange L, Jäggi A, Beutler G, Dach R, Mervart L (2009) Gravity field determination at the AIUB–the celestial mechanics approach. In: Sideris M (ed) Observing our changing earth. IAG symposium, vol 133. Springer, Berlin, pp 353–362. doi:10.1007/978-3-540-85426-5_42

Reubelt T (2009) Harmonische Gravitationsfeldanalyse aus GPS-vermessenen kinematischen Bahnen niedrig fliegender Satelliten vom Typ CHAMP, GRACE und GOCE mit einem hoch aufösenden Beschleunigungsansatz. Deutsche Geodätische Kommission, C 632, Verlag der Bayerischen Akademie der Wissenschaften, Munich (in German)

Reubelt T, Austen G, Grafarend EW (2003) Harmonic analysis of the Earth's gravitational field by means of semi-continuous ephemerides of a low Earth orbiting GPS-tracked satellite. Case study: CHAMP. J Geod 77:257–278. doi:10.1007/s00190-003-0322-9

Reubelt T, Sneeuw N, Grafarend EW (2012) Comparison of kinematic orbit analysis methods for gravity field recovery. In: Sneeuw N et al. (eds) VII Hotine-Marussi symposium on mathematical geodesy. IAG symposium, vol 137. Springer, Berlin, pp 259–265. doi:10.1007/978-3-642-22078-4_39

Reubelt T, Baur O, Weigelt M, Roth M, Sneeuw N (2013) GOCE long-wavelength gravity field recovery from 1s-sampled kinematic orbits using the acceleration approach. In: IAG symposium, vol 141 (accepted)

Schneider M (1968) A general method of orbit determination. Library Translation 1279, Royal Aircraft Establishment, Ministry of Technology, Farnborough, England

Sneeuw N, van Gelderen M (1997) The polar gap. In: Sansò F, Rummel R (eds) Geodetic boundary value problems in view of the one centimeter geoid. Lecture notes earth science, vol 65, Springer, Berlin, pp 559–568. doi:10.1007/BFb0011717

Sośnica K, Thaller D, Jäggi A, Dach R, Beutler G (2012) Sensitivity of Lageos orbits to global gravity field models. Artif Satell 47:47–65. doi:10.2478/v10018-012-0013-y

Švehla D, Rothacher M (2002) Kinematic orbit determination of LEOs based on zero- or double-difference algorithms using simulated and real SST data. In: Adam J et al. (eds) Vistas for geodesy in the new millennium, IAG symposium, vol 125. Springer, Berlin, pp 322–328. doi:10.1007/978-3-662-04709-5_53

Švehla D, Rothacher M (2004) Two years of CHAMP kinematic orbits for geosciences. EGU General Assembly 2004, Geophysical Research Abstracts 6:EGU2004-06645

Tapley BD, Bettadpur S, Watkins M, Reigber C (2004) The gravity recovery and climate experiment: mission overview and early results. Geophys Res Lett 31:L09607. doi:10.1029/2004GL019920

Van Gelderen M, Koop R (1997) The use of degree variances in satellite gradiometry. J Geod 71:337–343. doi:10.1007/s001900050101

Weigelt M (2007) Global and local gravity field recovery from satellite-to-satellite tracking. PhD Thesis, University of Calgary

Weigelt M, van Dam T, Jäggi A, Prange L, Tourian M, Keller W, Sneeuw N (2013) Time-variable gravity signal in Greenland revealed by high-low satellite-to-satellite tracking. J Geophys Res Solid Earth 118:3848–3859. doi:10.1002/jgrb.50283

Welch PD (1967) The use of fast Fourier transform for the estimation of power spectra: a method based on time averaging over short, modified periodograms. IEEE Trans Audio Electroacoust 15:70–73. doi:10.1109/TAU.1967.1161901